Extending the 3D-battery concept - large areal ultrashort pulsed laser structuring of multilayered electrode coatings

Y. Sterzl*, W. Pfleging
Institute for Applied Materials (IAM-AWP), Karlsruhe Institute of Technology, P.O. Box 3640, 76021 Karlsruhe, Germany

ABSTRACT

In the presented study, the use of an ultrashort pulsed laser system with high average laser power up to 300 W and repetition rate in the MHz regime in combination with multilayer coating was evaluated regarding the processing of multidimensional structured silicon/graphite anodes. Line patterned composite graphite anodes with grooves of different aspect ratios were generated by variation of laser and process parameters like laser fluence, pulse overlap, and repetition rate. The perspective of laser process upscaling is discussed, and it was shown that an increasing number of scans almost linearly increases the ablation depth, while the ablation width stays constant. The structured graphite anodes were handed over to a second coating step, in which a silicon containing slurry was coated to create an electrode architecture with spatial separation of graphite and silicon in the plane of the electrode. The quality of the multiple coated electrodes was studied to define a structure geometry in which defect-free filling is achieved in the second coating process. The filling of the electrode in the multilayer coating showed a dependence in blade gap during coating and laser-generated structure aspect ratio.

Keywords: ultrashort pulsed laser ablation, lithium-ion battery, 3D battery, multilayer coating, process upscaling

1. INTRODUCTION

Increasing electrification, especially in the automotive sector, poses new challenges for the development of advanced energy storage systems in terms of their energy and power density, lifetime, manufacturing costs, and environmental compatibility. A significant increase in energy density can be achieved by reducing the amount of inactive material by using electrodes with areal capacities greater than 4 mAh cm^{-2} [1]. Electrodes with such high areal capacity can be realized by using thick electrodes with thicknesses exceeding the state-of-the-art of today's high energy electrodes (65-80 µm) [2]. The disadvantages of increasing energy density via increasing mass loading are that battery performance decreases with increasing film thickness as well as a change in distribution of binder material in the electrode due to binder migration during electrode manufacturing [3, 4]. The usage of materials with high specific capacity, such as silicon on anode site, is another promising way to further increase the energy density due to a magnitude higher specific capacity of silicon (Si, 3579 mAh g^{-1}) compared to today commonly used graphite (Gr, 372 mAh g^{-1}) [5]. One drawback of Si is the large volume extension during lithiation of up to 280 % [6]. The volume expansion during electrochemical cycling leads to a delamination of the active material from the current collector, which in turn accelerates the capacity fade of the cell [7]. Furthermore, the Si particles can exceed the critical fracture toughness due to the stresses induced during the volume change, which leads to crack formation and crack propagation [8]. Electrode parameters such as porosity, tortuosity, layer thickness, type of active material and additives, as well as the electrode architecture (e.g., particle size distribution, porosity, topography) significantly influence the electrochemical performance of the cell [9]. A controlled adjustment of the electrode architecture can solve the mentioned drawbacks of increasing the energy density in the thick film concept and the capacity fade using Si as anode active material. Such a targeted adjustment of the electrode architecture can be realized, for instance, by laser ablation and multilayer coating.

Zheng et al.[10] structured a grid pattern with a structure pitch of 100 µm in 75 µm thick Si/Gr composite anodes (20 wt.% Si, 60 wt.% Gr, 10 wt.% carbon black) by ultrashort pulsed laser ablation. Half cells with structured and unstructured reference electrodes had a specific capacity of 700 mAh g^{-1} at a C-rate of C/5, but while the cells with structured electrodes could obtain a specific capacity of 650 mAh g^{-1} at a C-rate of 2C the unstructured showed a strong capacity fade with a specific capacity < 200 mAh g^{-1}. The post-mortem analysis of the dissembled cells after cycling showed crack formation in the electrode layer and deformation of the current collector in the unstructured electrodes, which were both not present in the structured electrode. Zheng et al attributes the observed defects to the mechanical stress inside the electrode during cycling, which can be reduced due to the laser generated free space.

*yannic.sterzl@kit.edu; phone +49 721 608-28161

With the concept of multilayer coating, it is possible to create a variation in porosity [11, 12], a distribution of active material and inactive material [13], as well as a spatial separation of several active materials in the electrode layer [14].

Müller et al [11] manufactured bi-layered graphite electrodes with a low porosity layer with a porosity of 32.5 % facing the current collector and a high porosity layer with a porosity of 73 % facing the separator and compared them to single layered electrodes with the respective porosity. Pouch cells with NMC 622 cathodes and double layered anodes showed a higher capacity retention at long term cycling at C-rates of C/3, C/2 and 1C compared to pouch cells with single layered anodes of similar areal capacity (3.09 mAh cm^{-2}). The pouch cells with single layered anodes reached a state-of-health (SoH) of 80 % after around 100 cycles, while the pouch cells with double layered anodes reached a SoH of 80 % after 600 cycles.

In the present study, the concept of multilayer coating and laser structuring is combined to generate multidimensional multimaterial anodes for lithium ion batteries. Particular attention was paid to process control and large-area laser structuring. Composite graphite anodes were laser structured and handed over to a second coating step, in which a silicon containing slurry was coated to create an electrode architecture with spatial separation of graphite and silicon in the plane of the electrode. The schematic manufacturing process is shown in Figure 1.

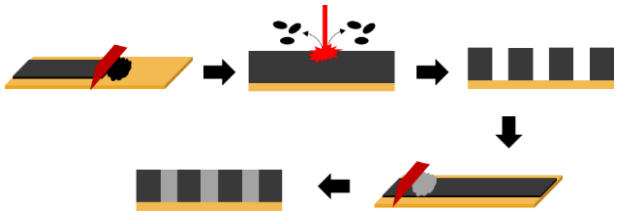

Figure 1. Schematic drawing of the alternating laser structuring and electrode coating for electrodes with spatial separation of active material in the plane of the electrode.

2. METHODOLOGY

2.1 Electrode manufacturing

A water-based 2 wt.% sodium caboxymethyl cellulose (CMC, MTI Corporation, USA) solution was prepared using a vacuum mixer (MSK-SFM-7, MTI Corporation, USA) and subsequently stirred for 24 h using a magnetic stirrer. Graphite (Gr, SPGPT808, Targray Inc., Canada), conductive carbon black (CB, C-nergy Super C65, Imerys G&C, Switzerland) and CMC solution was mixed with a dissolver (Labordissolver DB13, DISTECH GmbH, Germany) for 2.5 h and the solid content of the anode slurry was adjusted to 43 wt.% by adding deionized water. After homogenization of the slurry a styrene-butadiene rubber solution (SBR, MTI Corporation, USA) with a solid content of 50 wt.% was added and slowly stirred into the mixture. The slurry was doctor blade coated on a copper current collector (9 µm thickness, EQ-bccf-9u-180, MTI Corporation, USA) and dried at ambient temperature. The silicon-graphite slurry for subsequently coating of the graphite electrodes was prepared via ball milling. Graphite, conductive CB, silicon nano powder and CMC solution were premixed with a centrifugal mixer (Speedmixer DAC 150 SP, Hauschild, Germany). The slurry was subsequently processed with a ball mill (PULVERISETTE 7 premium line, Fritsch, Germany). SBR solution was added and stirred into the slurry with a centrifugal mixer. The composition of the electrode slurries is summarized in Table 1. For the process shown in Figure 1 the as prepared graphite anodes were laser structured and subsequently coated a second time with a silicon containing slurry. The quality of the multiple coated electrodes was examined by scanning electron microscopy to define a structure geometry in which defect free filling is achieved, and no electrode surface cracks are visible.

Table 1. Composition of electrode slurries.

Material	Graphite slurry	Silicon-graphite slurry
Graphite	93 wt.%	60 wt. %
Silicon	0 wt.%	30 wt. %
CB	1.4 wt.%	3.33 wt.%
CMC	1.87 wt.%	3.33 wt.%
SBR	3.73 wt.%	3.33 wt.%

2.2 Laser structuring

A high power, high repetition rate laser source (FX600-2-GFH, EdgeWave GmbH, Germany) with a maximum average power (P_{avg}) of 360 W, a pulse length of 600 fs, and a wavelength of 1030 nm was used to ablate the graphite electrodes. The beam radius at the laser exit is given as 1295 µm in x direction and 1373 µm in y-direction (M^2_x = 1.11; M^2_y = 1.07). The laser processing setup is shown in Figure 2 and consists of the laser source, a beam expansion telescope (BET) with a magnification of 6, a beam splitter which splits the beam in two separate beamlets which are guided to two galvo scanners (intelliSCAN III 20, SCANLAB GmbH, Germany) and respective F-theta lenses (JENar, JENOPTIK AG, Germany) each with a focal length of 255 mm. The calculated beam radii at the focus are 11.95 µm in x-direction and 10.85 µm in y-direction. The whole assembly is placed in a laser material processing system (MSV203 Laser Patterning Tool, M-SOLV LTD, UK) which is capable of roll-to-roll processing.

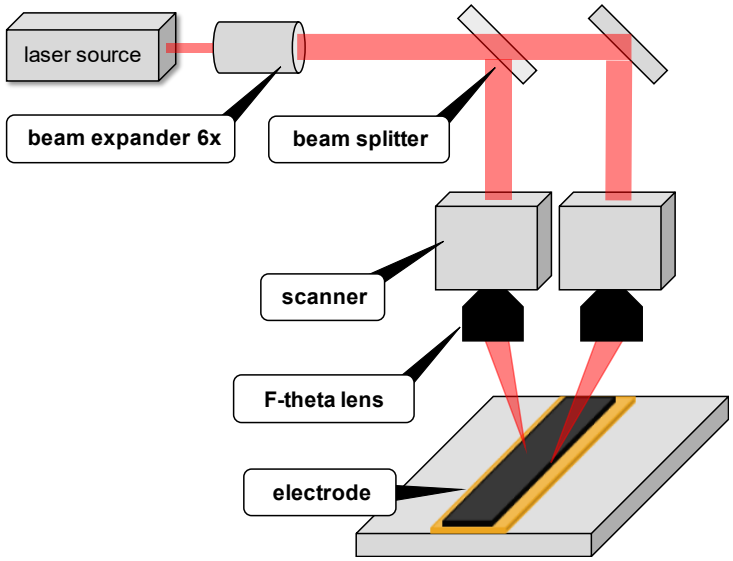

Figure 2. Schematic drawing of the used laser material processing system for large-area structuring of electrodes.

For a first investigation of the ablation behavior on anodes calendered to a porosity of 40 %, the pulse overlap was set constant and the number of passes (n), as well as the peak fluence (F_p) and repetition rate (f) were varied between 1-20 passes, 12-40 J cm^{-2}, and 100-1000 kHz, respectively. The scan speed for each repetition rate used is listed in Table 3. In a second step, the line energy (P_L) and with that the processing speed were set constant and n or v were varied to determine favorable processing strategies regarding a process upscaling. The ablation width at the top of the grooves and the ablation depth were measured using a digital microscope (VHX 7000, Keyence, Japan). For the multilayer electrodes, uncalendered electrodes were laser structured at a F_p of 18 J cm^{-2}, a v of 20 m s^{-1}, f of 1 MHz and an adjusted number of passes until the current collector has been reached. The width of the grooves was adjusted by multiple line scans at a line pitch of 30 µm.

Table 2. Applied repetition rate and scan speed for a constant pulse to pulse distance of 20 µm.

Repetition rate / kHz	**Scan speed / m s^{-1}**
1000	20
700	14
400	8
100	2

3. RESULTS AND DISCUSSION

3.1 Possible structure patterns and their capability of laser process upscaling

The structure pattern studied in these theoretical considerations are the most common patterns for electrode topography modification, namely the hexagonal hole pattern, the line pattern and the grid pattern. The pattern types are shown in Figure 3. The laser ablated material ("mass removal") determines the maximum amount of material which can be deposited in the electrode by the multilayer coating process described in Figure 1. The laser generated voids and respective mass removal for each type of pattern is a function of the structure pitch (p_s) and the structure dimension namely the width (w) of the holes and grooves, considering cylindrical shaped holes and rectangular shaped grooves. The mass removal as a function of p_s and w for each pattern type are listed in Table 3. The different design patterns were further evaluated by keeping the mass removal constant. The mass removal as a function of p_s for each pattern type with a similar structure diameter of 30 µm is shown in Figure 4 a). It comes clear that the hexagonal hole structure allows the smallest pitch distance and the grid structure the highest if the mass removal is kept constant. For a mass removal of 15 % one would have to set the pitch of the hole structure to 74 µm, for the line structure to 200 µm and for the grid structure to 384 µm.

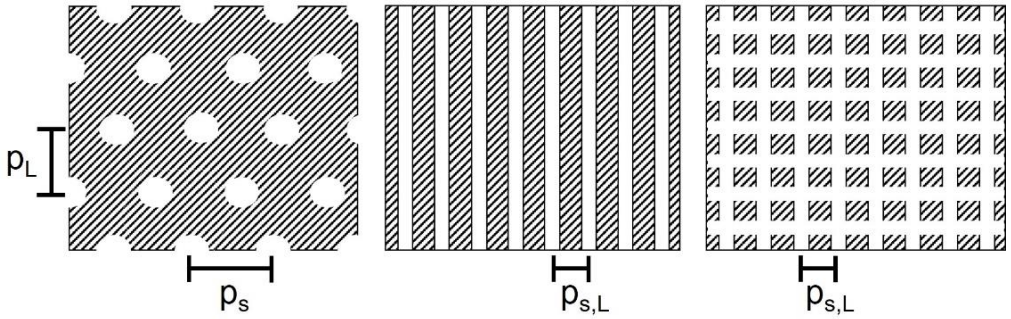

Figure 3. Schematic hexagonal hole pattern (left), line pattern (middle) and grid pattern (right) with structure pitch (p_s) and laser pitch (p_L).

When it comes to the implementation of the laser structuring into the industrial cell manufacturing, one have to pay attention to the processing speed, which should ideally match the belt speed in the production line (approx. 30-80 m min^{-1}) [15]. The hexagonal arranged hole pattern can be realized by two processing strategies. One is to drill one hole after another to the current collector, which comes along with disadvantages in the achievable processing speed due to the repeated acceleration and deceleration processes [16]. Another way is to drill the holes either in one or multiple passes of a line scan with a matched scanning speed and repetition rate to adjust the hole pitch. For the latter method and for the structuring of the line and grid pattern, the processing speed is a function of p_L, v, electrode dimension (l) and n, if the jump time between p_L is neglected.

Table 3. Mass removal and processing speed as a function of pattern type

Pattern type	Mass removal / %	Processing speed / m min^{-1}
Hex. hole pattern	$\frac{2\pi\left(\frac{w}{2}\right)^2}{\sqrt{3}p_s^2}\cdot 100$	$\frac{p_L v}{nl}\cdot 60$
Line pattern	$\frac{w}{p_s}\cdot 100$	$\frac{p_L v}{nl}\cdot 60$
Grid pattern	$\left(\frac{2w}{p_s}-\frac{w^2}{p_s^2}\right)\cdot 100$	$\frac{p_L v}{2nl}\cdot 60$

The calculated processing speed for a considered single pass ablation for each pattern with a mass removal of 15 % and an electrode dimension of 20 cm is shown in Figure 4 b). High scanning speeds of several hundred m s^{-1} are needed to reach a processing speed of >30 m s^{-1}. For the hexagonal hole pattern, a scanning speed of 1560 m s^{-1} would be required to reach

a processing speed of 30 m s^{-1}, while for the line pattern a scanning speed of 500 m s^{-1} would be sufficient. These high needed scanning speeds come along with the requirement of high repetition rates in the MHz regime to ensure a reasonable pulse overlap at the ablation of grooves or to adjust an adequate structure pitch for the hexagonal hole pattern. The demand of high scanning speeds could also be further reduced by multi-spot processing realized using diffractive optical elements. Feasibility and potential of process upscaling for high power laser structuring at repetition rates > 5 MHz, beam shaping, and splitting were already demonstrated in previous studies [17]

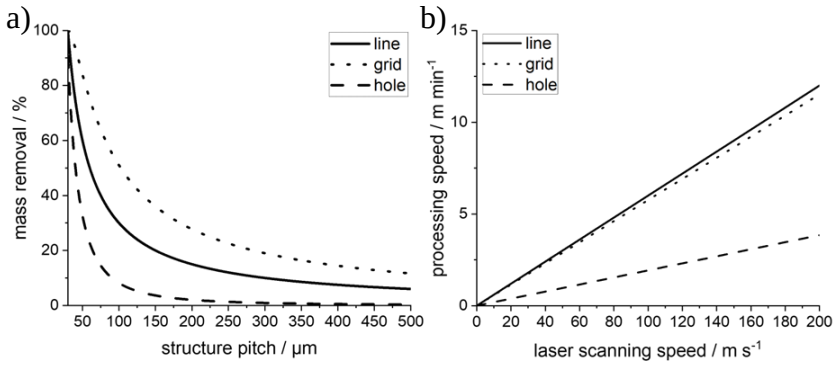

Figure 4. (a) Mass removal as a function of structure pitch (w=30 µm). (b) Processing speed as a function of laser scanning speed for single pass ablation (mass removal 15 %; l=20 cm, w=30 µm).

3.2 Investigation of the ablation behavior

With the previously made considerations it becomes clear that the line pattern is to be preferred with regard of achievable processing speed at reasonable scanning speeds. F_p, f, v, as well as n are processing parameters which determine the ablation depth and width of the laser structured grooves. For the multilayer coating process shown in Figure 1 an accurate knowledge of the ablation behavior is important to adjust the mass removal and groove geometry to the process. To study the ablation behavior of the composite graphite electrode, the ratio between v and f was set constant and the ablation depth and width was studied depending on F_p and f. In Figure 5 the ablation depth and width as a function of the logarithmic F_p is shown in Figure 5 for various f. With increasing F_p the ablation depth and width increase. At all F_p, a dependency of the ablation depth and width on f is observed. An increase in f from 100 kHz to 1 MHz comes along with a decrease in ablation depth and an increase in ablation width, more pronounces with increasing F_p. At a F_p of 40 J cm^{-2}, which corresponds to a pulse energy of 81 µJ, the ablation depth decreases from 75 µm at 100 kHz to 52 µm at 1 MHz, while the ablation width increases from 59 µm at 100 kHz to 78 µm at 1 MHz. This ablation behavior has also been observed in other work and may be associated with particle shielding effects [17, 18].

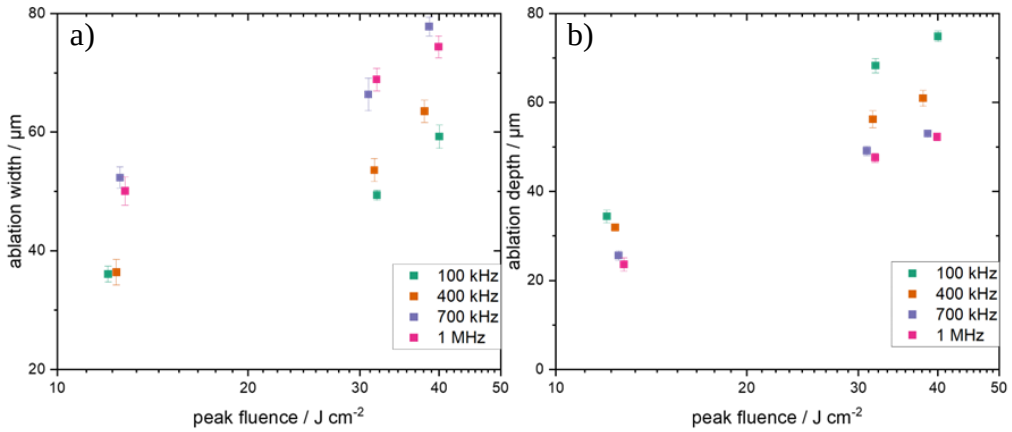

Figure 5. Ablation width (a) and depth (b) as a function of peak fluence F_p at several f (f=100-1000 kHz; n=10).

In terms of energetic efficiency of the process, it is reasonable to look at the ablation behavior as a function of line energy P_L. P_L is the ratio of P_{avg} and v multiplied with n. One could increase P_L by simply increasing n, or one could use a single scan and decrease v and with that increase the pulse overlap. If P_{avg} and the ratio between n and v is set constant, the latter two ablation strategies can be compared in terms of ablation efficiency. In Figure 6 the ablation depth and width as a function of P_L is shown. f and P_{avg} was set to 1 MHz and 26.1 W respectively. Keeping the pulse to pulse distance constant at 20 µm and increasing n (Figure 6, green) the ablation depth nearly linearly increases with P_L, while the ablation width stays at about 50 µm. For the single pass ablation, the ablation depth and width increase with increasing P_L. Compared with multi-pass ablation of same P_L, the ablation depth reached with single pass ablation is significantly higher. For a line energy of 26.06 J m^{-1} the ablation depth reached in single pass ablation (v = 1 m s^{-1}) is 67 µm, while for multi-pass ablation (v=20 ms^{-1}, n=20) the ablation depth is 38 µm. From the previously made observations of the ablation behavior at constant pulse overlap at increasing F_p and f, one would consider that the shielding effects would be more pronounced with decreasing pulse to pulse distance. The higher ablation depth observed at decreasing pulse to pulse distances nevertheless may indicate a transition to a more thermal ablation behavior, which is more pronounced due to an increased heat accumulation at low pulse-to-pulse distances. From the results it can be concluded that an ablation strategy with small pulse overlap and high n get beneficial for achieving a high aspect ratio for the generated grooves. If the aspect ratio of the laser structured grooves only matters to a minor extent, an ablation strategy with increased pulse overlaps and less passes would be more efficient and faster in terms of processing speed since the reached ablation depths are higher compared to the multi pass ablation of same P_L.

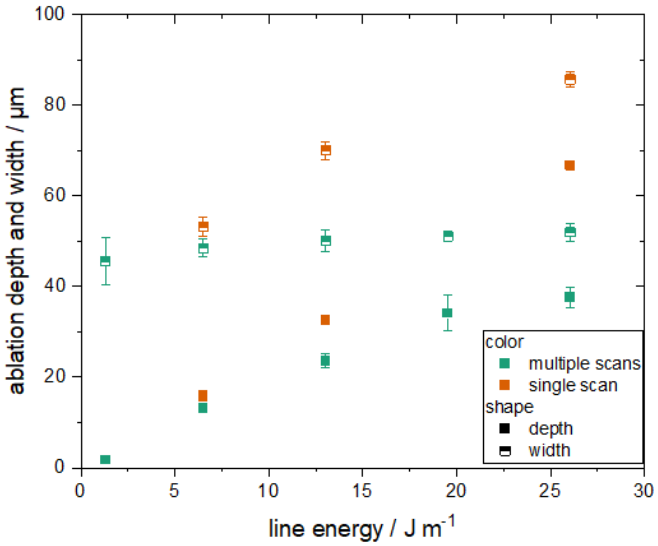

Figure 6. Comparison of the ablation depth and width as a function of $P_L = \frac{P_{avg}}{v} \cdot n$ of single pass (n=1, orange) and multi pass (n=1-20, green) ablation (laser parameter: 1 MHz and 26.1 W).

3.3 Multilayer coating of structured electrodes

The result for a multilayer coating for structures with a top width of 40 µm and 150 µm at blade gap a in contact mode, which represents a small blade gap almost in contact with the graphite electrode, is shown in Figure 7 a) and b). For both widths, filling with silicon slurry up to the current collector occurs. For grooves with a width of 40 µm, crack formation on top of the electrode is observed after the second coating, which are not apparent in the electrode with grooves of a width of 150 µm. It is very likely that the cracks are caused by induced tensile stresses in the coating due to shrinkage during drying. The filling height depends on the structure width and the blade gap during coating. Structures with a width of 40 µm coated with a larger blade gap show a nearly complete filling of the channels, while for broader structures no complete filling can be achieved. A possible explanation could be the higher capillary forces during the second coating due to the smaller width of the channels, which leads to a better wetting of the structures with slurry during coating. By

reducing the blade gap, the amount of material deposited on top of the electrode should be reduced and the induced tensile forces due to shrinkage should decrease. For the structures with a width of 40 µm coated at a small blade gap (Figure 7 c) no crack formation was visible and a reduced filling of the structures with silicon-based slurry, compared to the coating at a larger blade gap was observed. Figure 7 d) shows the result of the EDX measurement of a cross section of the electrode in Figure 7 c. A clear separation of the silicon-graphite domain and the pure graphite electrode can be observed inside the laser generated structure and on top of the electrode.

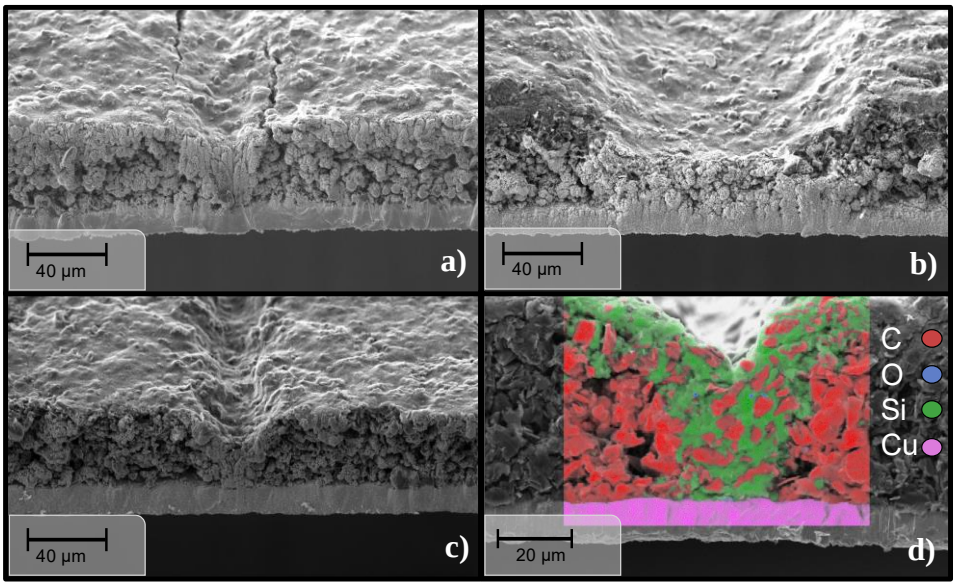

Figure 7. Scanning electron microscope images (a, b, c) and EDX measurement (d) of multilayer coated electrodes. Coated at large (a, b) and small blade gap (c, d).

4. CONCLUSION

A process strategy for the production of electrodes with spatial separation of graphite and silicon in the electrode plane was implemented by combination of large areal laser structuring and multilayer coating. The most used laser structure patterns in literature, namely the hexagonal arranged hole pattern, the line pattern, and the grid pattern were theoretical examined in terms of their process upscaling potential and it was shown, that for a similar mass removal the line pattern has the greatest potential in terms of achieving a high processing speed, which is necessary for a transfer of the laser structuring to the industrial battery production. Based on these theoretical considerations, the ablation behavior of graphite anodes was studied for line ablation. The ratio between the scanning speed and the repetition rate was set constant and the ablation depth and width was studied depending on the peak fluence and repetition rate. At all peak fluences, a dependency of the ablation depth and width on the repetition rate was observed, with decreasing ablation depth and increasing ablation width at increasing repetition rates. In terms of ablation efficiency two ablation strategies with same line energy were examined, the single pass ablation with increasing pulse overlap and the multiple pass ablation with increasing number of passes at constant pulse overlap. Ablation with a single pass showed a higher ablation depth and width compared to multi-pass ablation of same line energy. Graphite anodes were laser structured and subsequently coated a second time with a silicon containing slurry at two different blade gaps and the quality of the multiple coated electrodes was examined by scanning electron microscopy to define a structure geometry in which complete filling is achieved and no electrode surface cracks are visible. The filling of the electrode in the multilayer coating showed a dependence in blade gap during coating and structure aspect ratio. For structures with a width of 40 µm and a coating at a large blade gap a complete filling with silicon slurry, but also crack formation on top of the electrode was observed. Grooves coated at a decreased blade gap or broader grooves showed a less filling height, but no crack formation. With that the processing of defect free multidimensional multi-material electrodes by combination of laser structuring and multilayer coating was demonstrated.

5. ACKNOWLEDGEMENTS

We are grateful to our colleagues M. Kapitz and A. Reif for their technical assistance during laser processing and SEM measurements. This project has received funding from the German Research Foundation (DFG, project No. 467624762)

6. REFERENCES

[1] Pfleging, W., "Recent progress in laser texturing of battery materials: a review of tuning electrochemical performances, related material development, and prospects for large-scale manufacturing," Int. J. Extrem. Manuf. 3(1), 12002 (2021).

[2] Schmuch, R., Wagner, R., Hörpel, G., Placke, T. and Winter, M., "Performance and cost of materials for lithium-based rechargeable automotive batteries," Nat Energy 3(4), 267–278 (2018).

[3] Zhu, P., Seifert, H. J. and Pfleging, W., "The Ultrafast Laser Ablation of Li(Ni0.6Mn0.2Co0.2)O2 Electrodes with High Mass Loading," Applied Sciences 9(19), 4067 (2019).

[4] Park, J., Jeon, C., Kim, W., Bong, S.-J., Jeong, S. and Kim, H.-J., "Challenges, laser processing and electrochemical characteristics on application of ultra-thick electrode for high-energy lithium-ion battery," Journal of Power Sources 482, 228948 (2021).

[5] Obrovac, M. N. and Christensen, L., "Structural Changes in Silicon Anodes during Lithium Insertion/Extraction," Electrochem. Solid-State Lett. 7(5), A93 (2004).

[6] Obrovac, M. N. and Krause, L. J., "Reversible Cycling of Crystalline Silicon Powder," J. Electrochem. Soc. 154(2), A103 (2007).

[7] Wu, H. and Cui, Y., "Designing nanostructured Si anodes for high energy lithium ion batteries," Nano Today 7(5), 414–429 (2012).

[8] Graetz, J., Ahn, C. C., Yazami, R. and Fultz, B., "Highly Reversible Lithium Storage in Nanostructured Silicon," Electrochem. Solid-State Lett. 6(9), A194 (2003).

[9] Weiss, M., Ruess, R., Kasnatscheew, J., Levartovsky, Y., Levy, N. R., Minnmann, P., Stolz, L., Waldmann, T., Wohlfahrt-Mehrens, M., Aurbach, D., Winter, M., Ein-Eli, Y. and Janek, J., "Fast Charging of Lithium-Ion Batteries: A Review of Materials Aspects," Advanced Energy Materials 11(33), 2101126 (2021).

[10] Zheng, Y., Seifert, H. J., Shi, H., Zhang, Y., Kübel, C. and Pfleging, W., "3D silicon/graphite composite electrodes for high-energy lithium-ion batteries," Electrochimica Acta 317, 502–508 (2019).

[11] Müller, D., Fill, A. and Birke, K. P., "Cycling of Double-Layered Graphite Anodes in Pouch-Cells," Batteries 8(3), 22 (2022).

[12] Adrian Yao, [ELECTROCHEMICAL CELLS HAVING IMPROVED IONIC CONDUCTIVITY] (US 2021/0013498 A1), https://patentimages.storage.googleapis.com/77/fb/fd/ef4977eb097067/US20210013498A1.pdf (3 April 2022).

[13] Diehm, R., Kumberg, J., Dörrer, C., Müller, M., Bauer, W., Scharfer, P. and Schabel, W., "In Situ Investigations of Simultaneous Two-Layer Slot Die Coating of Component-Graded Anodes for Improved High-Energy Li-Ion Batteries," Energy Technology 8(5), 1901251 (2020).

[14] Song, Z., Zhu, P., Pfleging, W. and Sun, J., “Electrochemical Performance of Thick-Film Li(Ni0.6Mn0.2Co0.2)O2 Cathode with Hierarchic Structures and Laser Ablation,“ Nanomaterials 11(11), 2962 (2021).
[15] Kwade, A., Haselrieder, W., Leithoff, R., Modlinger, A., Dietrich, F. and Droeder, K., “Current status and challenges for automotive battery production technologies,“ Nat Energy 3(4), 290–300 (2018).
[16] Habedank, J. B., Schwab, D., Kiesbauer, B. and Zaeh, M. F., “Paving the way for industrial ultrafast laser structuring of lithium-ion battery electrodes by increasing the scanning accuracy,“ Journal of Laser Applications 32(2), 22053 (2020).
[17] A. Meyer, Y. Sterzl, S. Xiao, U. Rädel and W. Pfleging, “Ablation behavior of electrode materials during high power and high repetition rate laser structuring,“ 11989, 123–132 (2022).
[18] Habedank, J. B., Endres, J., Schmitz, P., Zaeh, M. F. and Huber, H. P., “Femtosecond laser structuring of graphite anodes for improved lithium-ion batteries: Ablation characteristics and process design,“ Journal of Laser Applications 30(3), 32205 (2018).